Critical comparison of experimental and computational fluid dynamic (CFD) results for a sample introduction system in plasma spectrometry

Elke Fasch[1*], Hermann Maier[2], Franz Landertshamer[3], Christian Weiß[1], Thomas Prohaska[1] and Wolfhard Wegscheider[1]

*elke.fasch@unileoben.ac.at
[1] Montanuniversität Leoben, Department General, Analytical and Physical Chemistry, Chair of General and Analytical Chemistry, 8700 Leoben, Austria
[2] gridlab GmbH – Optimisation & CFD, 8020 Graz, Austria
[3] HTBLuVA Salzburg, 5020 Salzburg, Austria
[4] Montanuniversität Leoben, Department of Environmental and Energy Process Engineering, Chair of Process Technology and Environmental Protection, 8700 Leoben, Austria

Introduction

The main task of a sample introduction unit for liquid samples is to modify the aerosol emitted by the nebulizer in terms of particle size, particle velocity and aerosol concentration.
A CFD (computational fluid dynamics) approach is used in a **parameter study of the dispersed flow in a Scott-type spray chamber** equipped with a micro-uptake glass concentric nebulizer (***Fig. 3***).

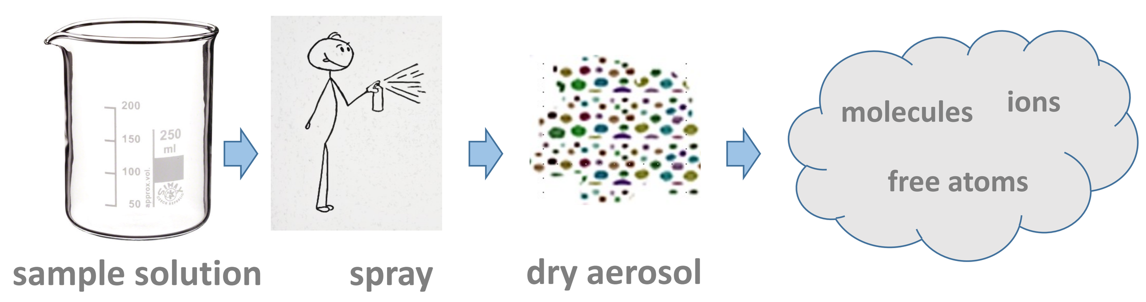

Fig. 1 *Processes when droplets enter the plasma*

Hypothesis:

- CFD can support to understand processes in the spray chamber.
- CFD is a substantial tool to possibly improve the design and size of spray chambers.

Methodology

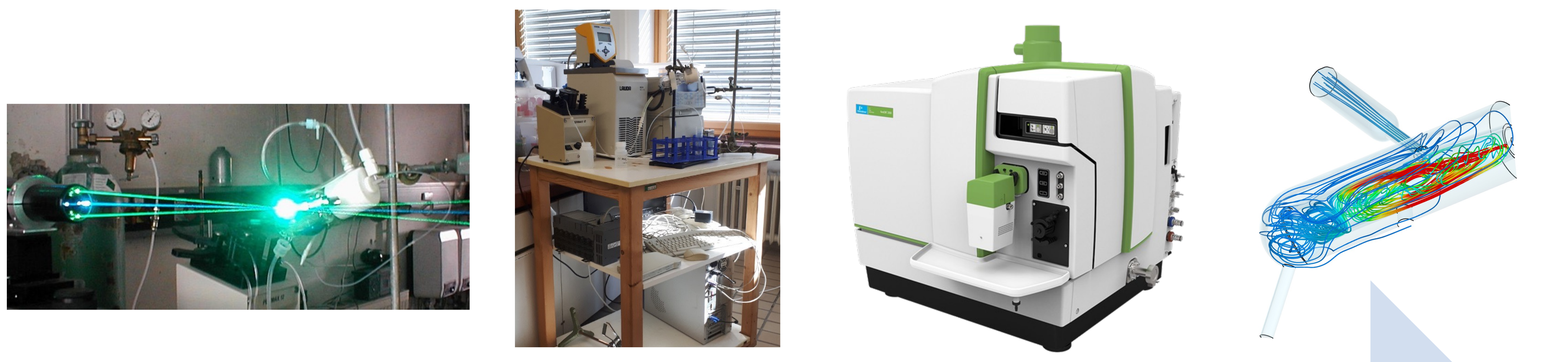

- Droplet size and velocity distribution measurements — Dual-beam phase-Doppler particle size analyser (Dantec, USA); Helos KR-Vario (Sympatec, Germany) High-Sped-PIV-Laser (Litron Lasers, England)
- Mass transport efficiency measurements — MicroMist 100 (Glass Expansion, Australia); Scott-type doube-pass spray chamber
- Analyte transport efficiency measurements — AHF CAL-7 NexION 2000B (PerkinElmer, USA)
- Numerical model — FIRE™ (AVL, Graz)

Numerical model

- Pre-processing
  - ⇨ Modules
  - ✓ Species (Ar, H_2O)
  - ✓ Spray
  - ✓ Thin Walls
  - ✓ Wallfilm
  - ✓ Turbulence: k-ζ-f

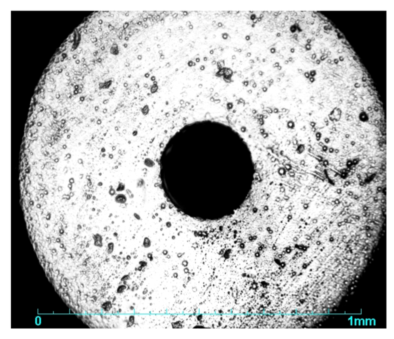

Fig. 2 *Nebulizer nozzle*

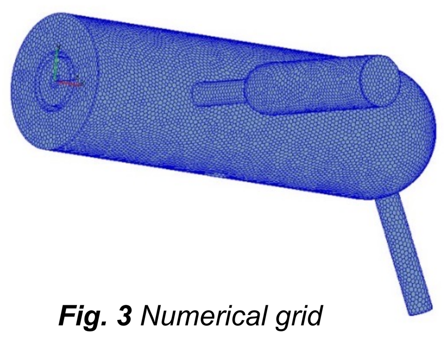

Fig. 3 *Numerical grid*

AVL FIRE®

Injected fluid:	water (20°C)
Spray angle:	20°
Nozzle diameter:	271 µm
Liquid flow:	110 µL min^{-1}
Argon flow:	0.8 L min^{-1}
T_{Ar}, nozzle exit:	-53.4°C
v_{Ar}, nozzle exit:	276 m s^{-1}
Numerical grid: ~245 000 cells	

Flow field – Argon jet (*Fig. 4 – Fig. 10*)

Turbulence due to shear forces between the nebulizer gas jet and the relatively static gas outside the free jet boundary generates large eddies near the nebulizer nozzle (see ***Fig. 4*** and ***Fig. 6***) and along the inner tube of the spray chamber, where most of the kinetic energy of the turbulent flow is concentrated.

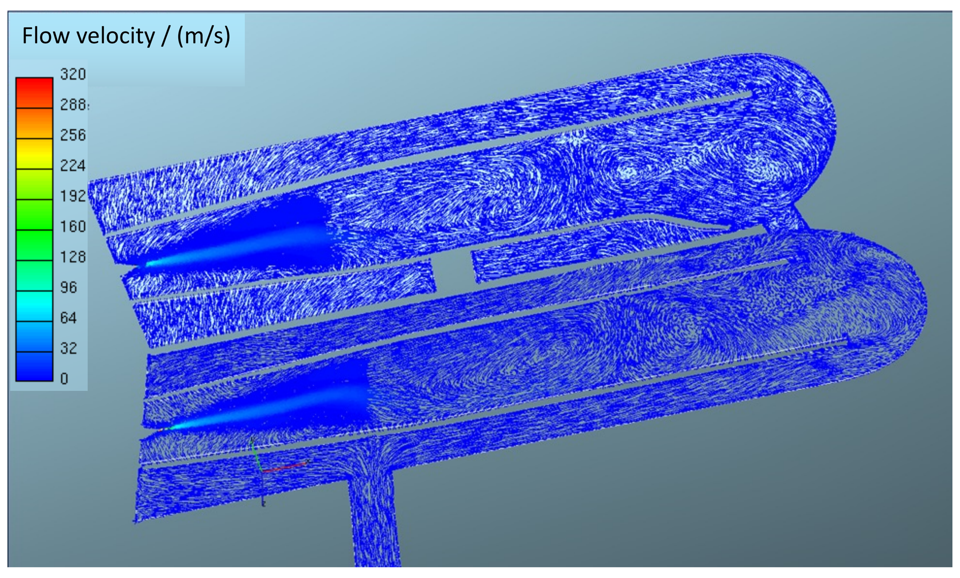

Fig. 4 *Velocity vector field in the Scott spray chamber*

The resulting flow performs a rotating pendulum motion around the jet axis (***Fig. 5***). After a flow reversal at the end of the inner cylinder of the Scott chamber, the turbulent flow becomes laminar and finally leaves the chamber in the direction of the plasma (***Fig. 7***).

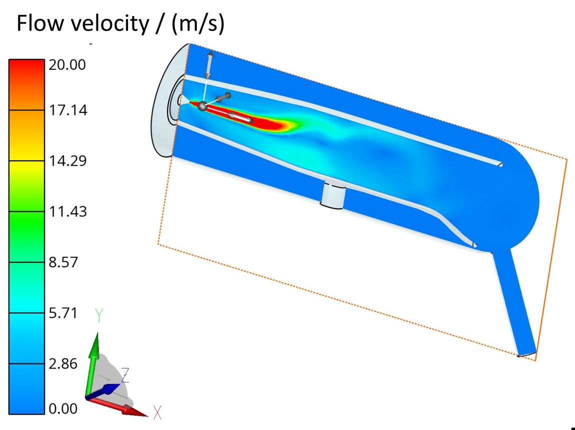

Fig. 5 *Velocity field at 6.5 s*

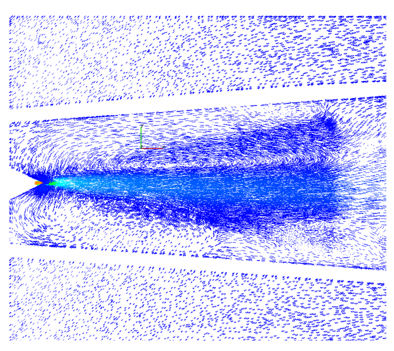

Fig. 6 *Velocity vector field near the nebulizer nozzle*

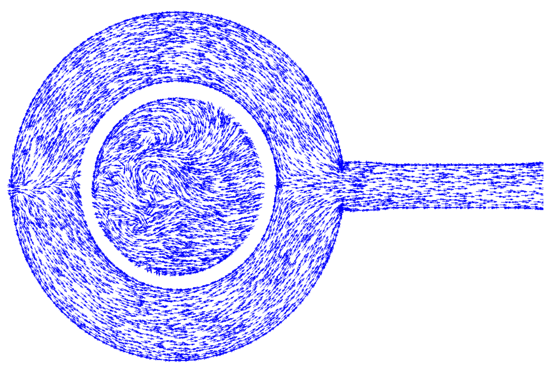

Fig. 7 *Turbulent velocity field in the inner tube of the spray chamber; laminar flow regime at the outlet of the spray chamber*

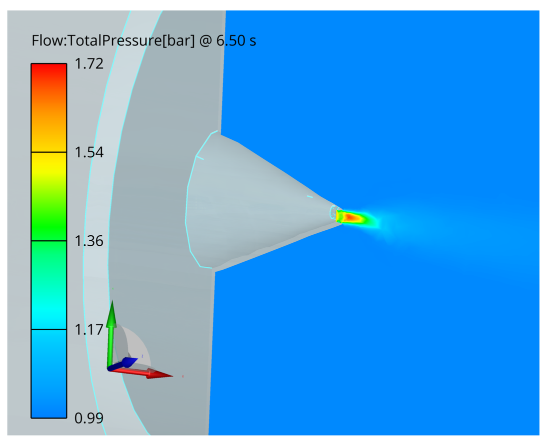

Fig. 8 *Pressure field in the inlet regime of the Scott spray chamber at 6.5 s*

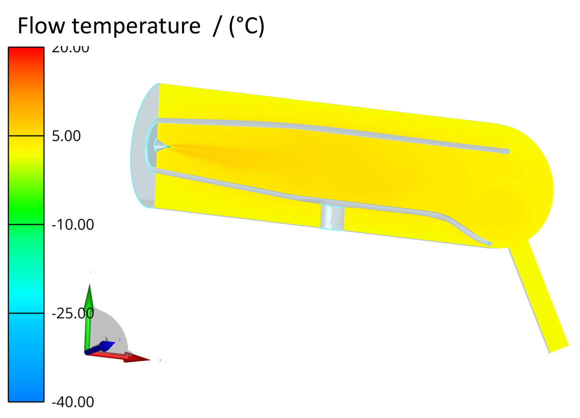

Fig. 9 *Temperature distribution in the Scott spray chamber thermostated at 2°C*

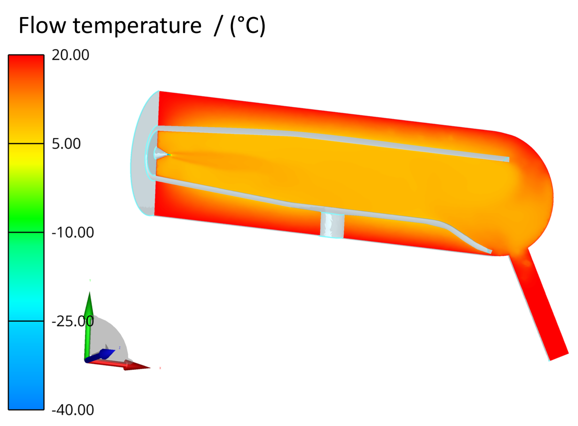

Fig. 10 *Temperature distribution in the Scott spray chamber thermostated at 20°C*

Droplet phase (*Fig. 11 – Fig. 17*)

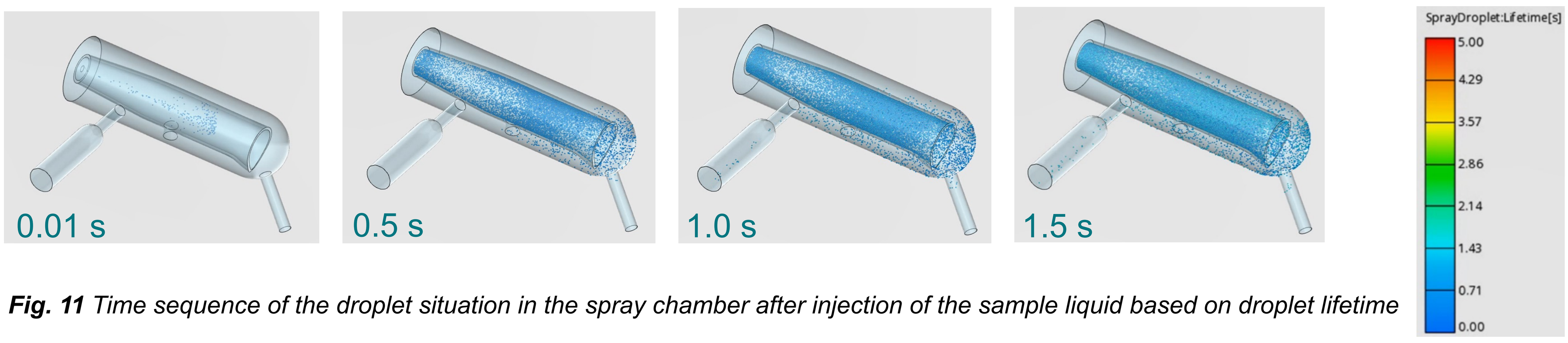

Fig. 11 *Time sequence of the droplet situation in the spray chamber after injection of the sample liquid based on droplet lifetime*

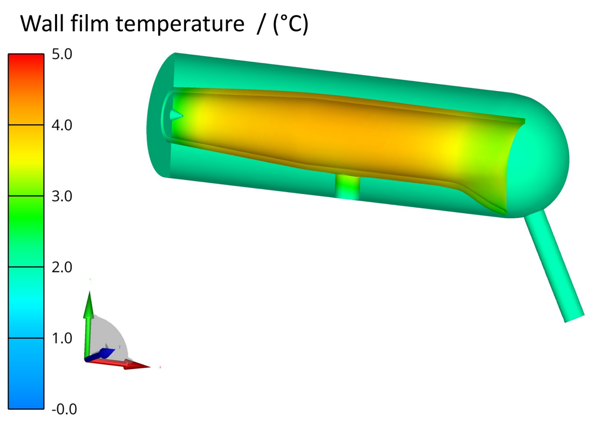

Fig. 12 *Wall film temperature of the spray chamber thermostated at 2°C*

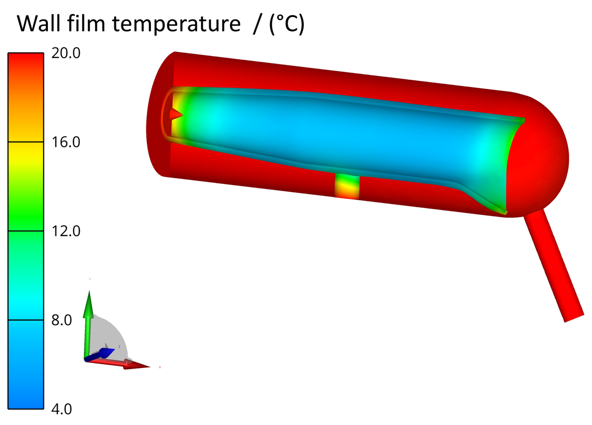

Fig. 13 *Wall film temperature of the spray chamber thermostated at 20°C*

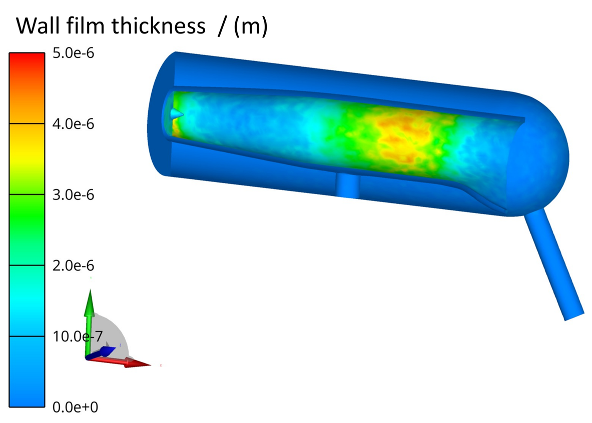

Fig. 14 *Wall film thickness*

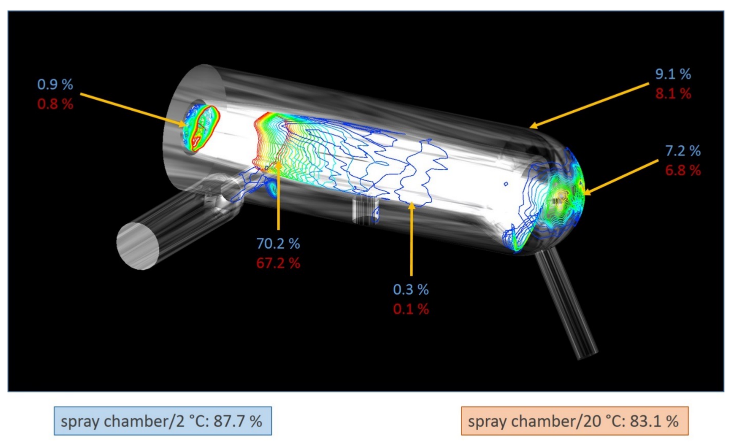

Fig. 15 *Deposition rates of the originally generated aerosol related to different areas in the spray chamber*

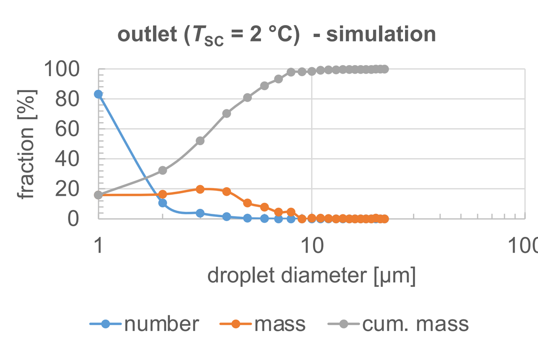

Fig. 16 *Calculated volume (mass) - based droplet size distributions of the aerosol leaving the Scott chamber (tertiary aerosol) thermostated at 2°C*

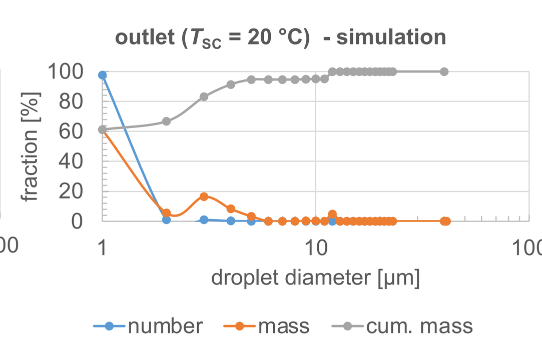

Fig. 17 *Calculated volume (mass) - based droplet size distributions of the aerosol leaving the Scott chamber (tertiary aerosol) thermostated at 20°C*

Validation of the numerical model (*Fig. 18 – Fig. 20*)

Fig. 18 *Zones of droplet impact nebulizing a methylene red solution*

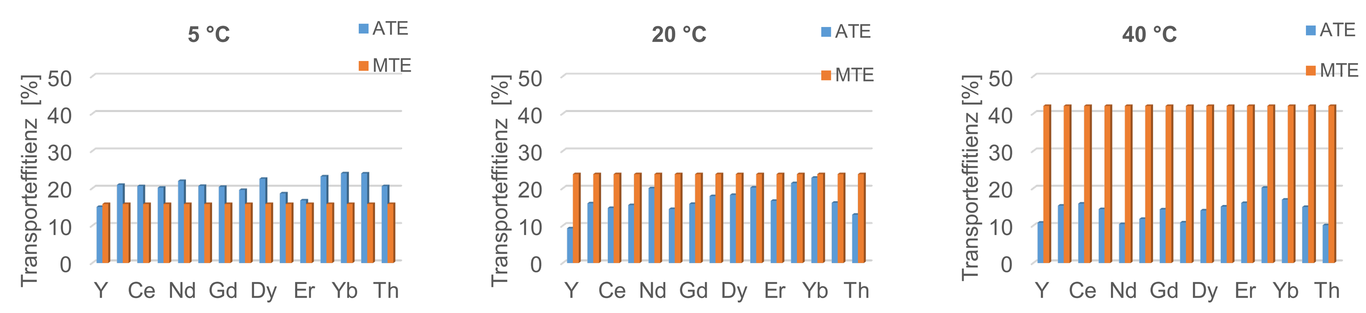

Fig. 19 *Mass transport efficiencies (MTE) vs analyte transport efficiencies (ATE) at different spray chamber temperatures*

Temperature Scott chamber	2°C Simulation	Experiment	20°C Simulation	Experiment
Mass transport	11 %	12% ± 1 %	16 %	20 % ± 3 %
Sauter diameter	2.1 µm	2.2 µm	1.2 µm	1.4 µm
dvol97	7.8 µm	8.3 µm	10.4 µm	9.1 µm
Velocity (plasma outlet)	1.0 m s^{-1}	0.8 m s^{-1}	1.0 m s^{-1}	0.8 m s^{-1}

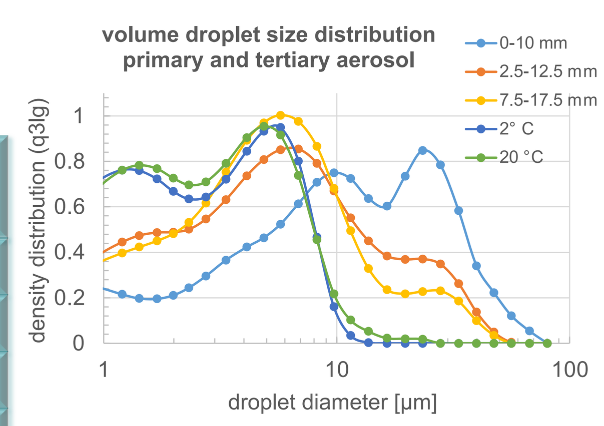

Fig. 20 *Volume based droplet size distributions*

Conclusions

- The results of the numerical calculations provide an approximation of the transport phenomena occurring inside the chamber and confirm the tendency that only a small amount of droplets is able to reach the plasma in relation to the injected liquid.
- Considering different conditions in the spray chamber, it can be seen that chamber cooling leads to a better performance of the sample introduction system as the solvent plasma load is reduced.
- Basically, the results of the simulations indicate that the deposition behavior in the spray chamber is determined by the flow field of the gas phase.
- Due to the fine aerosol and the low liquid flow rate, aerosol evaporation plays a key role in aerosol modification processes.